

Asymmetric Sawtooth Microstructure Induced Vapor Mobility for Suppressed Buoyancy Conditions: Terrestrial Experiment and Design for ISS Experiments

Karthekeyan Sridhar, *Student Member, IEEE*, Vinod Narayanan, and Sushil H. Bhavnani, *Member, IEEE*

1

Abstract— The lack of buoyancy forces in microgravity stagnates vapor bubbles on heated electronic surfaces, raising local surface temperatures above device operating limits. Though flow boiling can help dissipate higher heat fluxes, the addition of pumps and regulated flow loops increases design complexity for electronic systems. Passive directional motion of the fluid using an asymmetric sawtooth microstructure has demonstrated motion along the surface due to viscous forces. The current study explores the sawtooth microstructure in the nucleate boiling regime for a horizontal upward-facing and downward-facing orientation with varying sawtooth profiles (60°-30° and 75°-15°) in terrestrial gravity conditions as a precursor to ISS experiments. A laser powder bed fusion metal additive manufacturing technique was used to fabricate the test surfaces with 250 μm nucleation sites located on the long slopes. For the test surface with cavities spaced 2mm apart, the wall superheat was ~4K lower compared to cavities spaced 1mm apart in the upward-facing orientation. The downward-facing surface induced passive vapor mobility in the direction of the long slope, and a thin liquid film was observed between the vapor mass and microstructure. This liquid film thickness was predicted using a simplified force balance model modified from a prior parabolic flight experiment. The model predicted a uniform liquid film thickness of 49 μm for a vapor slug moving at 13.7 mm/s with the input heat flux at 1.25 W/cm². These terrestrial tests in the adverse orientation suggest that the sawtooth microstructure will successfully induce vapor mobility in upcoming ISS microgravity experiments. Elements of the final flight ampoule including the cooling zone, the two-stage pressure relief system and the high-speed imagery setup are discussed.

Index Terms—passive vapor mobility, microgravity, electronic thermal management, two-phase

ACRONYMS	
ASCENT	Asymmetric Sawtooth and Cavity-Enhanced Nucleation- Driven Transport
EDM	Electric Discharge Machining
FBCE	Flow Boiling and Condensation Experiment
ISS	International Space Station

This paper was submitted for review on February 28, 2021. Financial assistance for the project was provided by NSF under grant number 1740515.

K. Sridhar and S.H. Bhavnani are with the Department of Mechanical Engineering, Auburn University, Auburn, AL 36849 USA (e-mail:kzs0097@auburn.edu)

MSG	Microgravity Science Glovebox
NPBX	Nucleate Pool Boiling Experiment
ONB	Onset of Nucleate Boiling
PFMI	Pore Formation and Mobility during Controlled Directional Solidification in a Microgravity Environment Investigation

NOMENCLATURE

D	bubble departure diameter (m)
f	bubble frequency (Hz)
F	Force (N)
g	gravitational acceleration constant (m/s ²)
L	length (m)
P	pressure (atm)
r	radius of curvature (m)
R	bubble radius (m)
T	temperature (K)
V	velocity (m/s)

GREEK SYMBOLS

μm	micrometer or micron (10^{-6})
ΔP	Pressure drop (atm)
θ	Sawtooth angle (deg)
μ	dynamic viscosity (N-s/m ²)
σ	surface tension (N/m)
ρ	density (kg/m ³)

SUBSCRIPTS

d	drag
v	vapor
w	wall
sat	saturation

I. INTRODUCTION

Advancements in microelectronic fabrication have transitioned devices towards smaller form-factors,

V. Narayanan is with the Department of Mechanical and Aerospace Engineering, University of California Davis, Davis, CA 95616.

pushing the secondary engineering disciplines supporting this development towards dissipation of higher heat flux at improved efficiency and reliability. Thus, next-gen electronics require aggressive phase-change cooling techniques to maintain surface temperatures within operating limits. Dissipation of such high heat flux in microgravity conditions is especially challenging due to the lack of buoyancy that leads to stagnating vapor bubbles over the surface.

In microgravity environments, boiling from heated smooth and polished surfaces have produced stagnant, growing vapor bubbles. A drop tower experiment conducted by Xue et al. [1] led to the observation of two distinct modes of bubble growth and departure. When low heat flux is applied, large bubble grew on the surface with negligible coalescence. With increase in heat flux, more bubbles were produced with larger diameters. Thermocapillary forces sucked smaller vapor bubbles into large bubbles, subsequently leading to the departure of the larger vapor bubble as a result of the momentum from the coalescence. Similarly, Warrier et al. [2] observed, in the Nucleate Pool Boiling Experiment (NPBX), conducted by in the Microgravity Science glovebox (MSG) aboard the ISS, that bubbles merged together to form a central, large vapor bubble at low wall superheats. The studies cited above point to a consensus that vapor bubbles grow to large diameters in microgravity, creating a poor heat transfer situation on a heated surface. Some studies have explored the effect of bubble-based pumping for applications in microfluidics by different actuation mechanisms like thermal-based [3], acoustic-based [4] and optical radiation [5].

The present study details the terrestrial efforts to utilise repeating asymmetric microstructure to induce passive vapor mobility, in the run-up to microgravity experiments aboard the International Space Station (ISS). The work draws inspiration from a study by Linke et al. [6], who demonstrated passive motion of liquid droplets in the Leidenfrost regime by use of repeating millimetric-scale surface asymmetry in the form of 60°-30° ratchets. Kapsenberg et al.[7] added re-entrant cavities on the long slopes of 60°-30° sawtooth profile and demonstrated liquid motion parallel to the surface due to bubble growth. A parabolic flight experiment conducted with the sawtooth profile by Thiagarajan et al.[8] observed vapor bubbles sliding across the ratcheted microstructure in velocities upto 27.4 mm/s in microgravity flight experiments. The generated FC-72 vapor bubbles were also much larger than the bubbles observed in terrestrial gravity, similar to other microgravity experiments.

Terrestrial downward-facing surfaces can provide insight into the vapor bubble dynamics in microgravity as buoyancy forces do not assist in removal of vapor bubbles from the surface. Most Critical Heat Flux (CHF) models drop in accuracy when the downward-facing surface is included, indicating that a better understanding of the near-wall behaviors is needed [9]. A study conducted on the dynamics of the vapor slug in different orientations between 120° and 170° by Kim et al. [10] found that the translation speed of the sliding vapor slug was dependent on the size of the vapor slug and the orientation angle. A similar study with an inclined heater surface by Qiu and Dhir [11] led to the observation of a wedge-shaped liquid region between the vapor slug and the heated surface. The film thickness increased from the downstream side to the upstream

side of the vapor slug. Similar dynamics observed in the lower part of a horizontal tube by Kim et al. [12] resulted in a force balance model to account for the dominant forces that contribute to the sliding motion. While buoyancy, quasi-steady drag and added mass forces (from motion of the surrounding liquid) were dominant, the authors argued that the wake generated from a previous bubble might contribute to the motion and factored this correction in their model. For a bubble sliding upward in a narrow rectangular channel, Ren et al. [13] found that the drag force due to the difference in velocity between the bubble and liquid drove the sliding motion for decreasing bubble sizes.

The current study aims to explore the vapor bubble dynamics of the ratcheted microstructured surface with reentrant cavities for upward-facing and downward-facing orientations terrestrially to anticipate vapor bubble dynamics for the forthcoming ISS microgravity experiments. The ability to passively slide vapor bubbles across heated electronic surfaces without pumps or flow loops enables dissipation of high heat fluxes for next-gen electronics. Boiling curves were obtained for both orientations to predict the onset of nucleate boiling (ONB), wall superheat and dryout conditions. The experimental runs were conducted in a novel experimental setup that contained a borosilicate glass ampoule with circular-to-square transitions to mimic the available hardware for the microgravity experiments. The vapor bubble dynamics from the microstructure are compared with a flat, baseline surface for the downward-facing surface, and the presence of a thin liquid film between the microstructure and vapor slug was observed. A force balance model derived from an earlier Zero-G flight experiment in Thiagarajan et al.[8] was modified to predict the liquid film thickness for the downward-facing surface. The results from the terrestrial experiment are considered to design the final flight ampoule elements for the upcoming ISS experiments, including the transparent borosilicate glass ampoule, two-stage pressure relief system and Nichrome resistance heater. The obtained long-term microgravity data is expected to solidify the understanding of the vapor bubble dynamics from the sawtooth microstructure, and its feasibility as a passive electronic thermal management solution for spacecraft systems.

II. EXPERIMENTAL SETUP AND PROCEDURE

The test surface contained mirroring ratcheted section separated by a central, flat 20 mm section as shown in Figure 1. The footprint of the test surface is 120 mm x 6 mm x 2 mm (L x W x H). For the data reported in this study, a 50 mm section was heated to observe vapor bubble dynamics. The sawtooth profile varied between a 60°-30° structure and a 75°-15° structure. Nucleation sites with diameter of 250 μm nucleation sites were located on the long slope of the sawtooth. The test surfaces were manufactured using laser powder bed fusion, a metal additive manufacturing technique. Stainless steel (SS 316-L) surfaces were fabricated for the terrestrial reference experiments while titanium alloy (Ti-6Al-4V) test surface will be used for the microgravity experiments due to the close coefficient of thermal expansion (CTE) match to borosilicate glass. The stainless steel surfaces were electropolished in-house to obtain a smooth surface and mirror finish. The titanium alloy

surface were electropolished using a third-party vendor due to the safety hazards associated with the process.

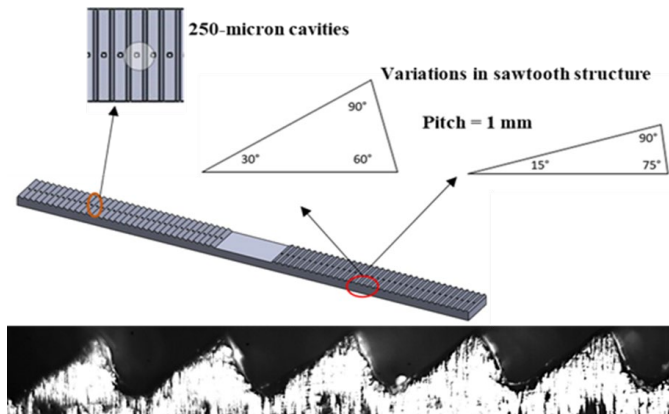


Figure 1 Details of additively manufactured test surfaces with differing sawtooth structures and 250 μm cavities (top). High-speed frame showing the sawtooth profile in focus (bottom)

Microgravity experiments aboard the ISS Laboratory will be performed in the Pore Formation and Mobility Investigation (PFMI) hardware [14]. Because the terrestrial experiments were conducted to anticipate vapor bubble dynamics in the upcoming ISS experiments, features of the experimental setup were adapted from the existing PFMI furnace ampoule. Though the methods of investigations of boiling phenomena in microgravity may vary, boiling experiments aboard the ISS have led to common experimental design features due to the concurrent need for compact form-factor and high-speed imaging. Subcooled flow boiling experiments were conducted by Sawada et al. [15] aboard the ISS using transparent pyrex glass tube to observe liquid-vapor dynamics and a heated copper tube to obtain local heat transfer coefficients. The resistive heater used on the pyrex glass was a thin gold film powered by brass electrodes at the ends of the tube. When both boiling and condensation are studied, the experimental design compounds in complexity with some common features. The Flow Boiling and Condensation Experiment (FBCE) [16] contains transparent polycarbonate plates for high-speed imaging and a heated wall consisting of 188 ohm resistors with glass passivation. The experiment contains six modules, including a test module assembly comprising the flow boiling module and the condensation module. The dielectric fluid normal-perfluorohexane is the test fluid, and a mass flow controller in the fluid module provides flow through the system.

The PFMI furnace, shown in Figure 2, can house an ampoule with an outer diameter of 12 mm and an overall length of 30 cm. The ampoule for the upcoming ISS experiments will contain two square-to-circular transitions. This unique geometry allows for ease of retrofitting in the existing PFMI hardware. A thin film of Nichrome will serve as the resistance

heater, with power delivered to this strip by two graphite electrode brushes from either end. The high-speed images for the flight experiment will be backlit through lighting provided from the flat face adjacent to the central heated section.

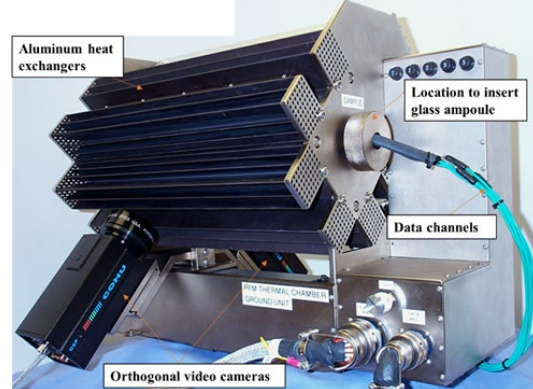


Figure 2 Feature of the PFMI furnace available for ISS experiments (adapted from [14])

The 80 mm test surface for the flight experiment will be carefully positioned in the glass ampoule to match the footprint of the deposited Nichrome film. The maximum heat input during the experiment is likely to be maintained under 5 W/cm², which is a power requirement that existing PFMI furnace can provide comfortably. The heater and cold zone details, camera translation stage and ampoule location is illustrated in the cross-section view of the PFMI furnace. A secondary cold zone will be added to the existing PFMI hardware, and the hypothesis shown in Figure 3(a) will be tested during the microgravity runs. The steep slope of the ratchet will face the ampoule sleeve, and the vapor bubble dynamics will be observed through high-speed imaging. Thermocouples will be placed at the surface, fluid and the two cold zones to provide perspective on the heat transfer characteristics of the microstructure. During the experimental runs, the cold zones will be maintained at the same heat removal rate to reduce any potential biases in fluid motion. When heat input is provided to the test surface, vapor is expected to be generated from the 250 μm nucleation sites as observed in the terrestrial experiment.

As the ampoule will be hermetically sealed during the experimental runs, a two- stage pressure relief system is being explored to offset the volume dilation due to vapor generation as shown in Figure 3(b). The primary stage will contain a flexible which can expand to accommodate the expanded volume. The secondary stage will contain Analytical Containment Transfer Tool (ACT2) media and can hold the entire volume of dielectric fluid (~23 ml) expected to be charged in the ampoule. This stage will safely contain potential leaks and prevent damage to the flight ampoules. The two-stage pressure relief system aims to maintain the pressure at near-constant levels during the experiment.

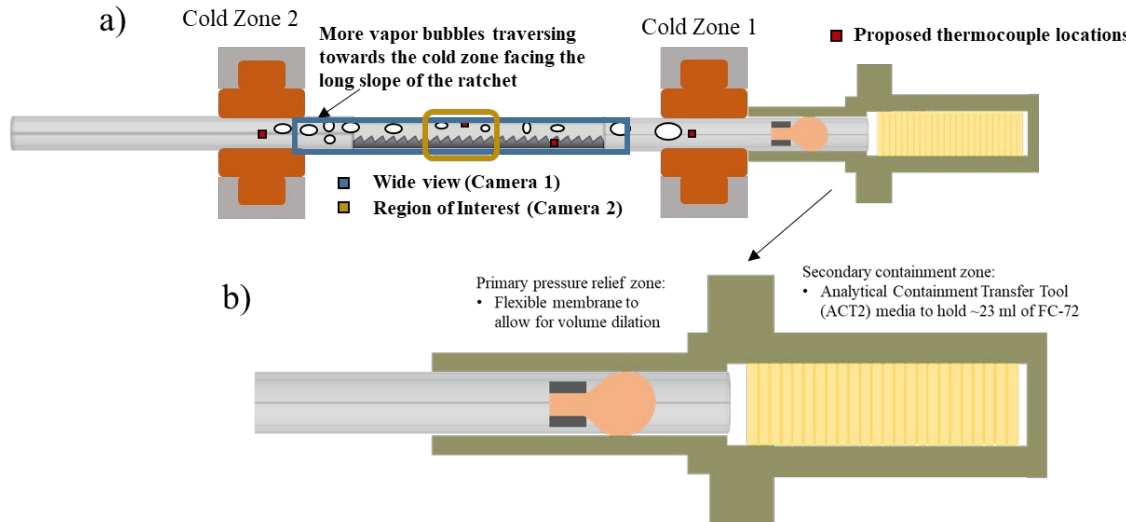


Figure 3 Schematic showing the hypothesis to be tested in the PFMI furnace aboard the ISS. Vapor bubbles from the nucleation sites are expected to preferentially move towards the cold zone facing the long slope of the ratchet. The proposed thermocouple locations are highlighted in the illustration at the surface, bulk fluid and the two cold zones. The frame of view for the two high-speed cameras is also illustrated 8b) The proposed two stage pressure relief system for the ISS microgravity experiments will contain a primary pressure relief and a secondary containment zone. The primary pressure relief zone will contain a flexible membrane to account for the volume dilation during the boiling process. The secondary containment zone will have ACT2 media to hold 23 ml of FC-72 dielectric fluid from the ampoule.

In the ISS experiment, the vapor bubble dynamics in the ampoule will be observed with two high-speed cameras, which will provide flexible frame of view. One of the high-speed cameras will be positioned to detail vapor bubble dynamics in a selected region of interest (ROI), while the other will capture the two-phase phenomenon in a larger area of the ampoule as illustrated in Figure 3. Both cameras will be mounted on translation stages to allow for flexible frame of view during the experimental runs.

As the terrestrial experiments were run to simulate the experimental conditions expected in ISS, important features of the PFMI hardware were recreated in the setup. A borosilicate glass ampoule was fabricated using glass-blowing techniques with two circular-to-square transitions, where the 12 mm circular profile was fused to the square cross-section with 8mm I.D and 1.2 mm wall thickness. The inlet port was used to pull vacuum and charge the dielectric fluid, while the access port was used to route the k-type thermocouples through the setup. Screw-top ports were added to the ampoule for test surface positioning, and the stainless steel bellows served as the pressure relief system for the closed system and helped set the degree of subcooling. Thermocouples were located at the surface and bulk fluid to obtain temperature data while the pressure transducer was located at the top of the bellows. Back-insulated polyimide film heaters were mounted on the glass ampoule to serve as the heat input for the test surface. The test surface was adhered to the ampoule using Arctic Silver thermal epoxy. The isometric view of the terrestrial experimental setup is shown in Figure 4.

A Phantom™ v310 camera outfitted with a K2/SC Infinity microscope lens was utilized for high-speed imaging in the terrestrial experiment. High-speed imaging was enabled through the unobstructed, flat face of the transparent ampoule, and the frame of view was backlit. LabVIEW™ was used to record the temperature and pressure data through interfacing with a data acquisition system in the terrestrial experiments. A

rope heater was wrapped around the bellows to maintain constant subcooling, and a Graham condenser was added to the top of the bellows during the degassing process. To dampen the influence of environment noise, like machinery vibration, the terrestrial experimental setup was housed on pneumatic vibration isolating feet (Newport™ SLM-1A).

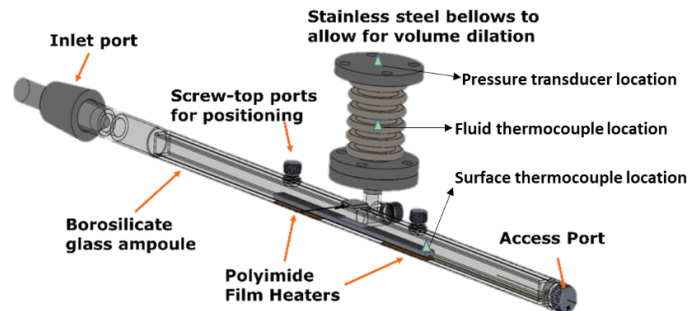


Figure 4 Isometric view of the complete ground experiment setup with positioning details of bellows and ports. The temperature and pressure measurement locations are highlighted.

The uncertainty in temperature measurement from calibrated Omega K-type thermocouples is ± 0.2 K. The uncertainty in bubble velocity and bubble frequency are estimated as $\pm 0.5\%$ and $\pm 5\%$ respectively. The uncertainty in pressure measurement from the pressure transducer (Omegadyne™ model no. PX319-050A5V) is $\pm 2\%$. The uncertainty in heat flux measurement for the range of reported values is $\pm 2\%$. A digital angle gauge calibrated to $\pm 0.1^\circ$ was used to level the tube for both orientations during the experimental runs.

III. EXPERIMENTAL RESULTS AND DISCUSSION

The parameters for the experimental study include test surface orientation (upward-facing and downward-facing) and effect of

nucleation site density (1-mm apart and 2-mm apart). Vapor bubble dynamics on baseline (flat) test surfaces were also observed to compare the effects of the sawtooth microstructure. The tests presented in this section were conducted at least twice to confirm repeatability. To reduce data redundancy and promote clarity of presented data, representative data are shown in each section below.

The dielectric liquid used for the terrestrial experiments is n-perfluorohexane (3M trade name FC-72). The subcooling for the data presented in the boiling curves is 20 K, while the initial pressure for the experimental runs in this section is under 1 atm.

Due to the unique geometry restriction in designing the terrestrial setup, the vapor bubble dynamics were heavily influenced by the liquid inventory afforded close to the surface as shown in Figure 5. At the start of the experimental run, the ampoule is flooded with dielectric liquid as the input heat flux is low. However, as the heat flux is increased and reaches the onset of nucleate boiling ($\sim 1 \text{ W/cm}^2$), vapor is generated from the nucleation sites on the microstructure. A liquid-vapor interface is created in the ampoule, and the generated vapor condenses in the bellows. At higher heat fluxes, more vapor is retained in the ampoule, eventually leading to dryout. The effect of this vapor production in the ampoule is more severe for the downward-facing surface as the generated vapor blankets the surface. Though the microstructure induces vapor mobility across the surface, the rapid vapor production at higher heat fluxes leads to premature dryout for the downward-facing surface. The dryout conditions for both test surface orientations are heavily influenced by the limited liquid inventory close to the surface.

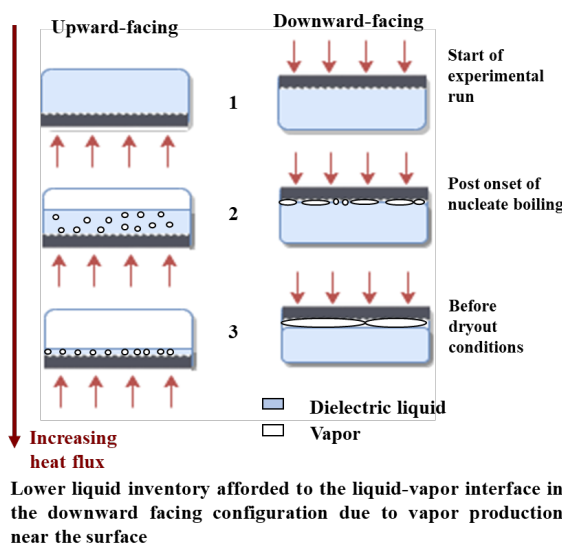


Figure 5 Vapor bubble dynamics in the square cross-sectioned ampoule for both orientations is illustrated in the figure. The low liquid inventory in the ampoule significantly influences the fluid dynamics at three distinct stages during the experimental runs.

The effect of test surface orientation significantly altered the boiling behavior as anticipated, as shown by the boiling curves in Figure 6. The onset of nucleate boiling occurred at a heat flux of 0.88 W/cm^2 for the downward-facing, significantly lower than the 1.1 W/cm^2 observed for the upward-facing surface. The wall superheat was also $\sim 3\text{K}$ lower for the downward-facing during the nucleate boiling process, and the dryout occurred at

2.5 W/cm^2 at this orientation. In contrast, the upward-facing surface reached dryout at 3 W/cm^2 and the wall superheat was maintained at $\sim 5 \text{ K}$ during the nucleate boiling process. The low wall superheat for the downward-facing surface is attributed to, in part, the efficacy of the microstructure in inducing passive vapor mobility across the surface.

The downward facing surface appears to be more effective in facilitating vapor mobility, causing a lower superheat during nucleate boiling. This advantage ceases when the vapor mass increases at higher heat flux leading to lower CHF values. This may be due to the increased vapor nucleation frequency at higher heat fluxes, leading to a rapid increase in the mass of vapor close to the surface. Quenching fluid is prevented from rewetting the surface, leading to dryout.

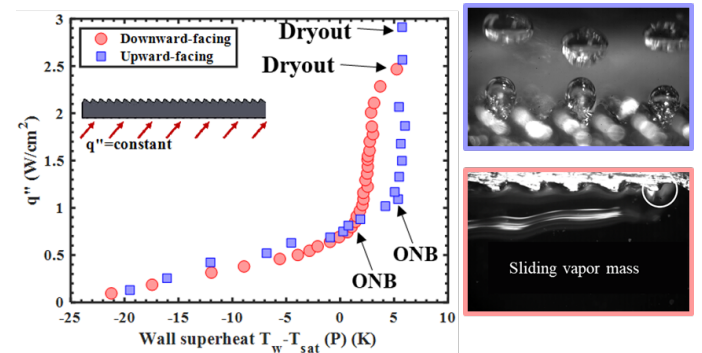


Figure 6 Wall superheat as a function of input heat flux for a 60° - 30° sawtooth test surface with cavities spaced 1-mm apart for the upward-facing surface and downward-facing surface.

A. Upward-facing surface

The vapor bubble morphology was measured from the high-speed images, and the pitch of the sawtooth (1 mm) was used to provide a length scale. Center of mass analysis was used to measure the velocity of the departing bubbles, with the assumption that the density of the vapor is uniform throughout the bubble. Image J [17] was used for all the image post-processing steps in the current study. The vapor bubble departure diameter was uniformly measured between 1 mm and 1.12 mm at a heat flux of 1.05 W/cm^2 , with no significant decrease in diameter within the frame of view. Similarly, the bubble velocity was in the range of 71 - 77 mm/s while the departure frequency was consistently resolved between 38 and 41 Hz . These vapor bubble parameters did not vary significantly in the range of input heat fluxes encountered in the upward-facing runs. An upward-facing surface with cavities spaced 2 mm apart is shown in Figure 7, with the frames used to obtain the image-processing parameters illustrated in a cutaway.

The bubble nucleates at an angle almost parallel to the sawtooth surface initially, and the bubble grows quickly to its departure diameter. In the later stages of bubble growth, buoyancy forces dominate and dictate the eventual departure direction.

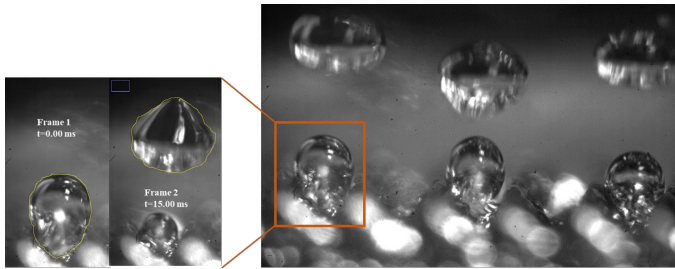


Figure 7 Bubble nucleation and departure from three 250-micron cavities on a 60°-30° sawtooth test surface with cavities spaced 2-mm apart. High-speed imaging is focused on the vapor bubbles to reduce distortion from fluid motion. (1280x800, 1000fps)

For the test surface with cavities spaced 2-mm apart, the wall superheat was ~4.5 K higher than the test surface with cavities spaced 1-mm apart as shown in Figure 8. This result validates the role of the 250 μm cavities as effective nucleation sites and is in line with expectations. In addition to significantly influencing the boiling curves, the nucleation site density also significantly affected the high-speed imagery. The test surface with cavities spaced 1-mm apart produced chaotic images due to fluid perturbation while the 2-mm spacing produced clear high-speed images.

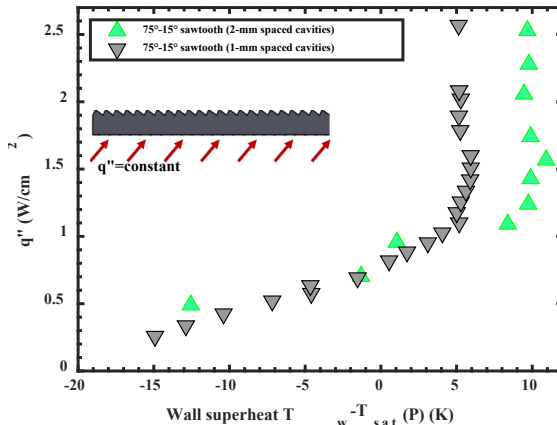


Figure 8 Effect of density of cavities on upward-facing surfaces with a 75°-15° sawtooth structure

B. Downward-facing surface

The flat baseline surface with no sawteeth produced large, stationary vapor bubbles that grew large enough to surpass the width of the test surface. Similar to the microstructured surface, the 250 μm nucleation sites were effective for the baseline surface as well, generating vapor bubbles consistently. The vapor bubble grew larger, coalescing with neighboring bubbles to form larger vapor bubbles. This continued process of growth and coalescence produced vapor bubbles large enough to exceed the test surface width and slide off in the z-plane (perpendicular to the direction of these images). The large vapor bubbles cause a dry patch underneath, raising local surface temperatures and causing premature dryout. This poor heat transfer situation can cause electronic components to fail at relatively low heat fluxes. Previous microgravity studies have suggested similar vapor bubble dynamics in microgravity, and the passive vapor mobility induced by the microstructure is expected to alleviate this problem. Another contrast between the microstructure and the baseline surface is the absence of the

thin liquid film on the flat test surface. Though high-speed imaging conditions were maintained similar to the sawtooth microstructure, image processing did not yield an observable liquid film for the baseline test surface.

Passive vapor mobility across the microstructure was observed with a 75°-15° sawtooth structure as shown in Figure 9. With the subcooling maintained at 20 K and the input heat flux at 1.25 W/cm², oblong vapor bubbles were generated from the 250 μm nucleation sites and grew large enough to fit their corresponding sawtooth profile. This growth led to coalescence with vapor bubbles generated from neighboring sawteeth. This initial stage of coalescence resulted in vapor slugs spanning across two or three sawteeth. These vapor slugs continued to grow and subsequently coalesced with each other to form a vapor mass large enough to cover four or five sawteeth. This vapor mass slid across the sawtooth microstructure in the direction of the long slope, disrupting the liquid-vapor boundary layer at the downstream edge. The dielectric liquid was observed to quench the test surface in its wake, and this sequence of nucleation, coalescence and the moving vapor mass was repeated.

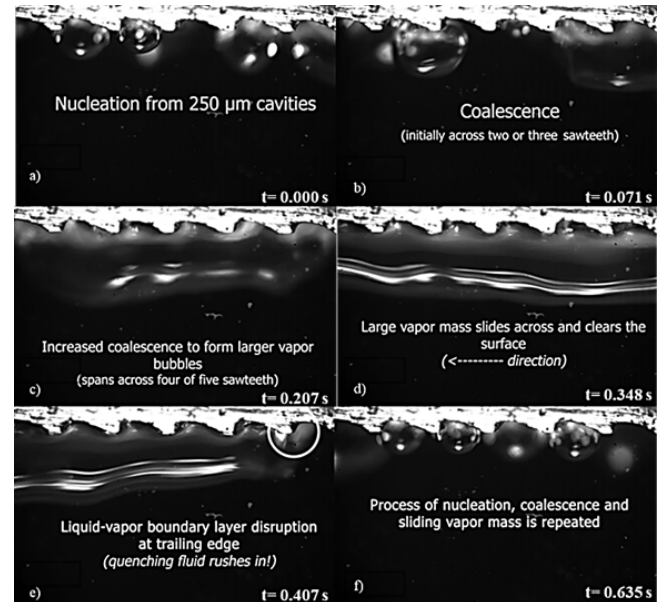


Figure 9 The sequence of images observed for the downward-facing surface is shown in the figure at an input heat flux of 1.25 W/cm² (20 K subcooling). Vapor bubbles nucleate from the 250 μm nucleation sites (a), and grow large enough to coalesce with neighboring vapor bubbles to form large vapor bubble spanning across two or three sawteeth (b). These larger vapor bubble continue to coalesce with each other to form a large vapor slug (c) that subsequently slides across and clears the surface in the direction of the long slope (d). The liquid-vapor boundary layer is disrupted at its trailing edge (e), allowing quenching fluid to rewet the surface. The three stages of nucleation, coalescence and sliding vapor mass is repeated when the heat flux is held constant.

In backlit imaging conditions, a liquid-vapor interface was observed close to the microstructure in an earlier study[18] when a quick-moving vapor slug covered the microstructure as shown in Figure 10. Image-processing pointed to the presence of a thin liquid film close to the surface, and the thickness of the liquid film was measured at the crest and trough of the sawteeth. For the 75°-15° sawtooth, measurements were possible at two heat fluxes. At a heat flux of 1.25 W/cm², the liquid film

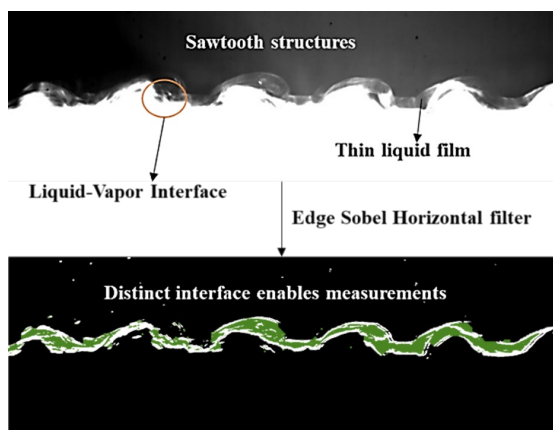


Figure 10 The liquid film observed between the microstructure and the vapor slug measured by applying the Edge Sobel Horizontal filter. The image on the bottom has been post-processed to highlight the thin liquid film.

C. Downward facing surface- Vapor transit model

The observations from the high-speed images that show a liquid film along the vapor slug and the microstructure can provide more insight to structure a force balance model. A prior parabolic flight experiment also observed a thin liquid film underneath a sliding bubble at 0.45 W/cm^2 in μg , and the authors [8] hypothesized that the pressure difference between the crest and trough of the sawtooth played a crucial role in the observed sliding motion. The force balance model based on this hypothesis has been modified to account for the downward-facing surface in this section. The schematic for the model is illustrated in Figure 11.

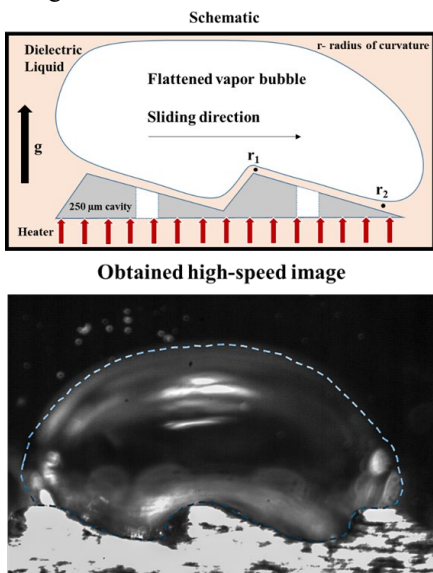


Figure 11 Illustration indicating the model parameters in the schematic and a representative high-speed image from the terrestrial downward-facing runs. Buoyancy forces are acting against the surface, as evidenced by the flipped gravity vector

The pressure drop along the sawtooth was expressed using the Young-Laplace equation, assuming that the pressure inside the vapor bubble is uniform. The radius of curvature at the crest (r_1) and trough (r_2) is illustrated in Figure 11.

$$P_{1,l} - P_{2,l} = 2\sigma \left(\frac{1}{r_1} + \frac{1}{r_2} \right) \quad (1)$$

where $P_{1,l}$ and $P_{2,l}$ are the pressure in the liquid at the crest and trough respectively and σ is the surface tension of the dielectric liquid (FC-72).

The liquid film flow between the microstructure and the vapor bubble can be hypothesized to be a fully developed planar Couette-Poiseuille flow with bubble moving at a constant velocity V . The horizontal component of the total shear force acting on the bubble along the shallow slope and steep slope of the sawtooth contributed to the total force due to pressure difference shown by

$$F_{\Delta P, tot} = \left\{ \begin{array}{l} m \left[\left(\frac{\mu V}{H} + \frac{H}{2} \frac{\partial P}{\partial x} \right) LW \cos \theta \right]_{\text{long slope}} \\ -n \left[\left(\frac{\mu V}{H} + \frac{H}{2} \frac{\partial P}{\partial x} \right) LW \sin \theta \right]_{\text{short slope}} \end{array} \right\} \quad (2)$$

where, $\frac{\partial P}{\partial x}$ is the pressure gradient between the crest and trough of the sawtooth, H is the liquid film thickness, θ is the angle of sawtooth and L is the length of the liquid film between the surface of saw tooth and vapor bubble. V is the constant velocity at which the vapor bubble is moving while W is the equivalent diameter of the vapor bubble. m and n are the number of long slopes and short slopes covered by the vapor slug respectively.

The inertial component of Stokes drag was included in the force balance as the vapor bubble moves through a pool of dielectric liquid (including the thin liquid film at the surface) expressed by

$$F_d = 4\pi\mu RV \quad (3)$$

where R is the radius of bubble ($R=W/2$).

The force due to nucleation from the cavities was not considered for parabolic flight experiments as the momentum transferred to the liquid was not expected to be a significant component in microgravity. However, the downward-facing surface showed consistent nucleation and coalescence from the $250 \mu\text{m}$ cavities, and the force was derived from a momentum balance given by Merte [19]. The model assumes that the energy from coalescence is ideally converted to kinetic energy in microgravity conditions, and is represented by

$$F_v = \pi \sum_{i=1}^k D_i^2 \bar{f}_i \sqrt{\frac{\sigma_i \rho_{v,i}}{3}} \quad (4)$$

where, \bar{f}_i is mean bubble departure frequency, D_i is the bubble departure diameter, σ_i is the surface tension and $\rho_{v,i}$ is the vapor density.

The total force balance for this model can be represented by

$$F_{\Delta P, tot} + F_v - F_d = 0 \quad (5)$$

In the current semi-empirical formulation of the force balance model, the force due to the pressure difference between the crest and trough of the sawteeth is an order of magnitude greater than the force due to nucleation from the cavities, suggesting that the asymmetric sawtooth microstructure is the primary driver of vapor mobility for the downward-facing surface.

Another modification to the microgravity model is the 75° - 15° sawtooth profile for the terrestrial study, contrasting the 60° - 30° sawtooth profile used in the parabolic flight

experiments. The input parameters for the model were obtained from processing consecutive high-speed images at a heat flux of 1.25 W/cm^2 and 1.78 W/cm^2 (shown in Table 1). The velocity of the vapor slug increased with input heat flux, suggesting that the microstructure might provide self-regulating thermal management. The fluid properties used in the model were obtained at the saturation temperature of FC-72.

Table 1 Input to the simplified model at a heat flux of 1.25 W/cm^2 and 1.78 W/cm^2

Parameter	$q=1.25 \text{ W/cm}^2$	$q=1.78 \text{ W/cm}^2$
Diameter (D)	0.0061m	0.0077m
r1	0.00028m	0.00029m
r2	0.00038m	0.00035m
Velocity (V)	13.7 mm/s	21.8 mm/s
Frequency (f)	6 Hz	11 Hz
No. of sawteeth covered by vapor slug	2	4

At a heat flux of 1.25 and 1.78 W/cm^2 , the model predicted a uniform liquid film thickness of $49 \mu\text{m}$ and $116 \mu\text{m}$ respectively. The corresponding liquid film thickness at these heat fluxes was obtained at the crest and trough through image processing for ten locations and compared with the predicted uniform thickness, as shown in Table 2.

Table 2 The measured liquid film thickness at the crest and trough compared with the predicted liquid film thickness from the modified model

Input Heat Flux (W/cm^2)	Average liquid film thickness at crest (μm)	Average liquid film thickness at trough (μm)	Liquid film thickness predicted by the modified model, H (μm)
1.25	46	124	49
1.78	74	180	116

An important assumption of the model is that the liquid layer thickness is uniform across the crest and trough of the sawtooth. The vapor mass transit model detailed above is an attempt at predicting the liquid film thickness for the downward-facing surface using force components derived from microgravity, bridging the suppressed buoyancy conditions for the vapor slug. However, the asymmetry in the liquid film between the crest and trough warrants further analysis at higher heat fluxes to validate the observed trend. The prediction of the liquid film thickness is crucial in enabling numerical simulations of the physics from the sawtooth microstructure in varying gravitational fields. The utility of the asymmetric sawtooth profile can potentially expand beyond electronics thermal management at different length-scales for retrofitting into system-level fluid applications. The upcoming ISS microgravity experiments labelled Asymmetric Sawtooth and Cavity-Enhanced Nucleation-Driven Transport (ASCENT),

will explore the viability of the vapor mobility from the microstructure in microgravity using an unique experimental setup.

ASCENT will explore different test surface to detail vapor bubble dynamics afforded by the microstructure in long-term microgravity conditions. The first test surface will contain $250 \mu\text{m}$ nucleation sites spaced 1-mm apart on a 60° - 30° sawtooth profile. To explore the effect of nucleation site density, the second test surface will have these cavities spaced 2-mm apart on the 60° - 30° sawtooth profile. The third test surface will contain $250 \mu\text{m}$ slot cavities on the 60° - 30° sawtooth profile and will be fabricated by Electric Discharge Machining (EDM). The fourth variation, a baseline flat surface with nucleation sites but no ratchets, is expected to quantify any asymmetries between the two cold zones in the PFMI furnace. The payload will carry redundant ampoules to offset possible defects in ampoule fabrication, assembly, and breakage.

Positioning the test surface non-intrusively during the assembly process is a current challenge for ASCENT. The metrics for success in the microgravity experiment will be quantified by consistent nucleation from the engineered sites and clear preferential motion towards the cold zone facing the long slope of the sawtooth. The ability to induce passive vapor mobility across heated electronic surfaces can enable high-heat flux dissipation for spacecraft systems.

IV. CONCLUSIONS

The terrestrial experimental setup was designed to mimic important features of the existing ISS-PFMI hardware, and the borosilicate glass ampoule limited the available liquid inventory to the surface, leading to dryout at 3 W/cm^2 for the upward-facing surface and $\sim 2.5 \text{ W/cm}^2$ for the downward-facing surface. The pressure difference between the crest and trough of the sawteeth induce passive vapor mobility in the direction of the long slope when buoyancy forces acted against the surface. High-speed images captured a thin liquid film between the vapor slug and the microstructure, and a modified force balance model predicted the liquid film thickness at two heat fluxes. A vapor slug moving at 13.7 mm/s at an input heat flux of 1.25 W/cm^2 was predicted to slide on a $49 \mu\text{m}$ liquid film by this force balance model. Nucleation site density significantly influenced the wall superheat for the upward-facing surface, as cavities spaced 1-mm apart maintained wall superheat $\sim 5 \text{ K}$ lower in contrast to cavities spaced 2 – mm apart. The experimental design of the upcoming ISS-ASCENT project will utilise a thin film of Nichrome to serve as the resistive heater and accommodate two square-to-circular transitions in the borosilicate glass ampoule for ease of retrofitting. A two-stage pressure relief system containing a primary zone with a flexible membrane and a secondary zone with ACT2 media to hold the entire volume of fluid in the ampoule. The microgravity experiments are expected to detail the vapor bubble dynamics from the microstructure and capture the preferential vapor mobility in the direction of the long slope. Vapor mobility from the microstructure across electronic heat sources in microgravity can enable next-gen electronics to maintain surface temperatures within operating limits.

ACKNOWLEDGMENT

Financial assistance for the project was provided by NSF under grant number 1740515. The authors thank Rachel Ormsby, George Tipker, Paul Faget, Ethan Davis, and Andy Kurk from Techshot (ASCENT's implementation partner) for sharing the experimental designs of the flight ampoule elements mentioned in the study.

REFERENCES

- [1] Y. F. Xue, J. F. Zhao, J. J. Wei, J. Li, D. Guo, and S. X. Wan, "Experimental study of nucleate pool boiling of FC-72 on smooth surface under microgravity," *Microgravity Sci. Technol.*, vol. 23, no. SUPPL. 1, 2011.
- [2] G. R. Warrier, V. K. Dhir, and D. F. Chao, "Nucleate pool boiling eXperiment (NPBX) in microgravity: International space station," *Int. J. Heat Mass Transf.*, vol. 83, pp. 781–798, 2015.
- [3] J. H. Tsai and L. Lin, "Active microfluidic mixer and gas bubble filter driven by thermal bubble micropump," 2002.
- [4] Y. Gao, M. Wu, Y. Lin, W. Zhao, and J. Xu, "Acoustic bubble-based bidirectional micropump," *Microfluid. Nanofluidics*, vol. 24, no. 4, p. 29, Apr. 2020.
- [5] B. A. Bezuglyi and N. A. Ivanova, "Pumping of a fluid through a microchannel by means of a bubble driven by a light beam," *Fluid Dyn.*, vol. 42, no. 1, pp. 91–96, Feb. 2007.
- [6] H. Linke *et al.*, "Self-propelled leidenfrost droplets," *Phys. Rev. Lett.*, vol. 96, no. 15, 2006.
- [7] F. Kapsenberg, N. Thiagarajan, V. Narayanan, and S. Bhavnani, "Lateral motion of bubbles from surfaces with mini ratchet topography modifications during pool boiling- experiments and preliminary model," *Intersoc. Conf. Therm. Thermomechanical Phenom. Electron. Syst. ITERM*, pp. 165–175, 2012.
- [8] N. Thiagarajan, S. H. Bhavnani, and V. Narayanan, "Self-propelled sliding bubble motion induced by surface microstructure in pool boiling of a dielectric fluid under microgravity," *J. Electron. Packag. Trans. ASME*, vol. 137, no. 2, 2015.
- [9] G. Liang and I. Mudawar, "Pool boiling critical heat flux (CHF) – Part 2: Assessment of models and correlations," *International Journal of Heat and Mass Transfer*, vol. 117. Elsevier Ltd, pp. 1368–1383, 01-Feb-2018.
- [10] J. M. Kim, J. H. Kim, and H. S. Ahn, "Hydrodynamics of nucleate boiling on downward surface with various orientation. Part I: Departure diameter, frequency, and escape speed of the slug," *Int. J. Heat Mass Transf.*, vol. 116, pp. 1341–1351, Jan. 2018.
- [11] D. Qiu and V. K. Dhir, "Experimental study of flow pattern and heat transfer associated with a bubble sliding on downward facing inclined surfaces," *Exp. Therm. Fluid Sci.*, vol. 26, no. 6–7, pp. 605–616, Aug. 2002.
- [12] J. S. Kim, Y. N. Kim, and H. K. Cho, "Predicting the sliding bubble velocity on the lower part of a horizontal tube heater under natural convection based on force balance analysis," *Int. J. Heat Mass Transf.*, vol. 151, p. 119453, Apr. 2020.
- [13] T. Ren, Z. Zhu, J. Shi, C. Yan, and R. Zhang, "Experimental study on bubble sliding for upward subcooled flow boiling in a narrow rectangular channel," *Int. J. Heat Mass Transf.*, vol. 152, p. 119489, May 2020.
- [14] R. A. Stivey, S. Gilley, A. Ostrogorsky, R. Grugel, G. Smith, and P. Luz, "SUBSA and PFMI transparent furnace systems currently in use in the International Space Station Microgravity Science Glovebox," 2003.
- [15] K. Sawada, T. Kurimoto, A. Okamoto, and S. Matsumoto, "Investigation of Dissolved Air Effects on Subcooled Flow Boiling Heat Transfer for Boiling Two-Phase Flow Experiment onboard the ISS," 2014.
- [16] J. Defiebre and M. Guzik, "Assembly and Integrated Systems Testing for the Flow Boiling and Condensation Experiment (FBCE)," 2019.
- [17] C. A. Schneider, W. S. Rasband, and K. W. Eliceiri, "NIH Image to ImageJ: 25 years of image analysis," *Nature Methods*, vol. 9, no. 7, pp. 671–675, Jul-2012.
- [18] K. Sridhar, R. Smith, V. Narayanan, and S. Bhavnani, "Phase

Change Cooling of Spacecraft Electronics: Terrestrial Reference Experiments Prior to ISS Microgravity Experiments," in *InterSociety Conference on Thermal and Thermomechanical Phenomena in Electronic Systems, ITERM*, 2020, vol. 2020-July, pp. 315–322.

- [19] H. Merte, "Momentum effects in steady nucleate pool boiling during microgravity," *Ann. N. Y. Acad. Sci.*, vol. 1027, pp. 196–216, 2004.



Karthekeyan Sridhar received the M.S. degree in mechanical engineering from Auburn University, Auburn, AL in 2020. He is currently pursuing the Ph.D. degree with the Department of Mechanical Engineering in Auburn University where he is a graduate research assistant at the Enhanced Heat Transfer Laboratory.

His research interests include two-phase heat transfer and electronics thermal management, with a focus on microgravity applications. He received the Master's Thesis award for 2020-2021 from Auburn University.



Vinod Narayanan is a Professor in the Department of Mechanical and Aerospace Engineering at UC Davis where he also serves as the Associate Director of the UC Davis Western Cooling Efficiency Center. He earned his PhD in 2001 from Texas A&M University. Prior to moving to UC Davis in 2015, he progressed through the ranks at Oregon State University. His group has contributed to literature in jet impingement heat transfer, infrared thermography applied to microscale thermal transport, passive phase-change thermal transport, and process intensification. He serves as an Associate Editor of ASME Journal of Thermal Science and Engineering Applications and is an ASME Fellow.



Sushil H. Bhavnani holds the Henry M. Burt Chair in Mechanical Engineering at Auburn University. His primary research area is in liquid cooling of high-powered microprocessors. He is a past recipient of the ASME Electrical and Electronics Packaging Division's Clock Award for sustained contributions to the area of electronics packaging. He has served as the General Chair of the Intersociety Conference on Thermal and Thermomechanical Phenomena in Electronic Systems (ITerm). He has authored over 160 refereed journal and conference publications resulting from research sponsored by agencies such as NASA, the National Science Foundation, Southern Company, the U. S. Department of Energy, and the U. S. Department of Defense. His teaching has been recognized with several excellence awards, including the Mortar Board Award, the Walker Award, the Birdsong Award, the Pumphrey Award, and the Leischuck Presidential Award for Excellence in Teaching. He is a Fellow of the American Society of Mechanical Engineers. Sushil has led student teams in international solar-powered car and solar house competitions and is the recipient of the 2020 Auburn University Outstanding Faculty Advisor Award.